THE IRIS SODIUM CELL INSTRUMENT

G. GREC, E. FOSSAT, B. GELLY, and F. X. SCHMIDER
Département d'Astrophysique, Université de Nice, 06034 Nice Cedex, France

(Received 19 February, 1990; in revised form 2 August, 1990)

Abstract. In the framework of the IRIS programme, full-disk solar Doppler-shift measurements are made with an optical resonance sodium cell spectrophotometer, a new pattern of the instrument successfully used at the geographic South Pole 10 years ago. After many successive improvements, the IRIS version has now become a precise and reliable device, being limited only by the solar and/or by the atmospheric noise in all the frequency ranges of interest for the *p*-mode and the *g*-mode investigation. This instrument is described here in some detail, with the technical specification for each individual component being defined by comparison to the photon and the solar noise.

1. Introduction, Principle

It is today known that solar oscillations exist on a broad spectrum. At one end, the oscillations with very long horizontal wavelength penetrate to the solar interior, down to the core if they are radial. At the other end, those with very short wavelength are mainly surface phenomena. The oscillations that exist inside the Sun correspond to different spherical modes of the solar body and have led to the development of helioseismology. As seismology provides information about the internal structure of the Earth, the measurement of several parameters (such as frequency, lifetime, rotational splitting, amplitude), although still successful only for the pressure modes, produces new insights about the solar interior.

If this seismic method has developed only recently in the case of the Sun, it is mainly because the amplitude of each wave at the visible surface is extremely small. The typical numbers are 10 to 20 m on the solar radius, or 1 to 2 mK in surface temperature, or 10 cm s^{-1} in upward or downward surface velocity. These coherent amplitudes must be looked for through a high level of 'solar noise' due to all kinds of random motions generated by the convection itself, such as granules and supergranules, or on longer time-scales by magnetic activity. In this context, experience has proved that the Doppler-shift measurement offers the best signal-to-noise ratio. On the other hand, it appears to be extremely difficult to measure micromagnitude or milliarc-sec through the Earth's atmosphere. As a consequence, most ground-based helioseismology instruments measure the Doppler shift of the solar light, with or without angular resolution.

The IRIS instrument measures the Doppler line-of-sight velocity spatially integrated over the total visible solar surface. It is then sensitive only to the very low degree modes ($l \leq 3$), which penetrate deep inside the solar core if they are pressure modes, and which are the only modes that can possibly reach the surface with significant amplitudes if they are gravity modes.

The Doppler signal is made up of a differential monochromatic photometric signal, the two spectral windows being located near the points of maximum slope on the two

Solar Physics **133:** 13–30, 1991.

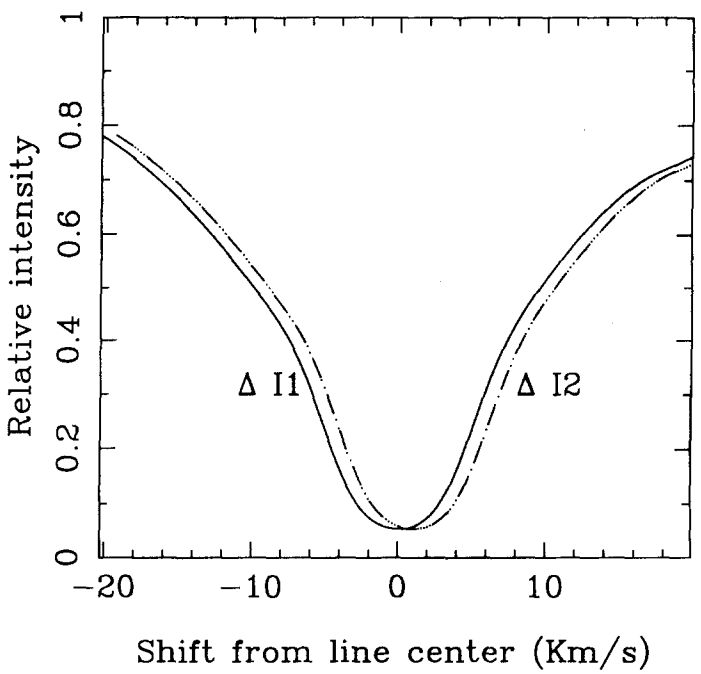

Fig. 1. Principle of Doppler shift measurement by means of differential monochromatic photometry. In the IRIS instrument, the 2 spectral windows are not symmetrically located with respect to the solar line axis, due to the astronomical radial velocities.

wings of the Na D1 5896 Fraunhofer line (Figure 1). The monochromator used is an optical resonance cell, which contains adequately heated and thermally controlled sodium vapour. The D1 absorption wavelength is split into the two needed components by means of the Zeeman effect produced by a transverse magnetic field of about 5 kG. In units of Doppler velocity, these two spectral windows are located at ± 5 km s^{-1} around the central D1 wavelength. Adding up the gravitational redshift and the radial velocity components of both the orbital and the spin earth motions (the solar oscillations are negligible here), the result never exceeds 1.5 km s^{-1}. Even taking into account the additional 2 km s^{-1} redshift of the western solar limb, the differential measurement produces then a signal which is a monotonic function of the line-of-sight velocity (the calibration procedure will be dealt with in another paper of this volume).

This instrument has been developed in our Department at the Nice University over about 20 years, and its principle has been described several times before (Fossat, 1970; Fossat and Roddier, 1971; Grec, Fossat, and Vernin, 1976). Similar instrumentations using the optical resonance in monoatomic vapours or beams have also been described, using potassium (Snider, 1970; Brookes, Isaak, and Van der Raay, 1978) or strontium (Blamont and Roddier, 1961; Roddier, 1965). Our sodium cell instrument was the first one to detect the 5-min oscillation integrated on the whole solar disk (Fossat and Ricort, 1973; Fossat, 1975) and the first one to make possible the identification of individual eigenmodes of the solar sphere (Grec, 1981; Grec, Fossat, and Pomerantz, 1980, 1983).

Many improvements have become necessary and have been possible since the last published description in 1976. This paper presents the technological choices which have been selected for the need of the IRIS network operation.

2. Description of the Instrument

The general optical scheme is shown in Figure 2, the principle of the electronic measurement in Figure 3.

The sunlight first goes through a 6-Å prefilter, then is focused at 40 cm by a 3.5 cm diameter simple lens (L1). A field diaphragm of 1.5 solar diameter is located there, and

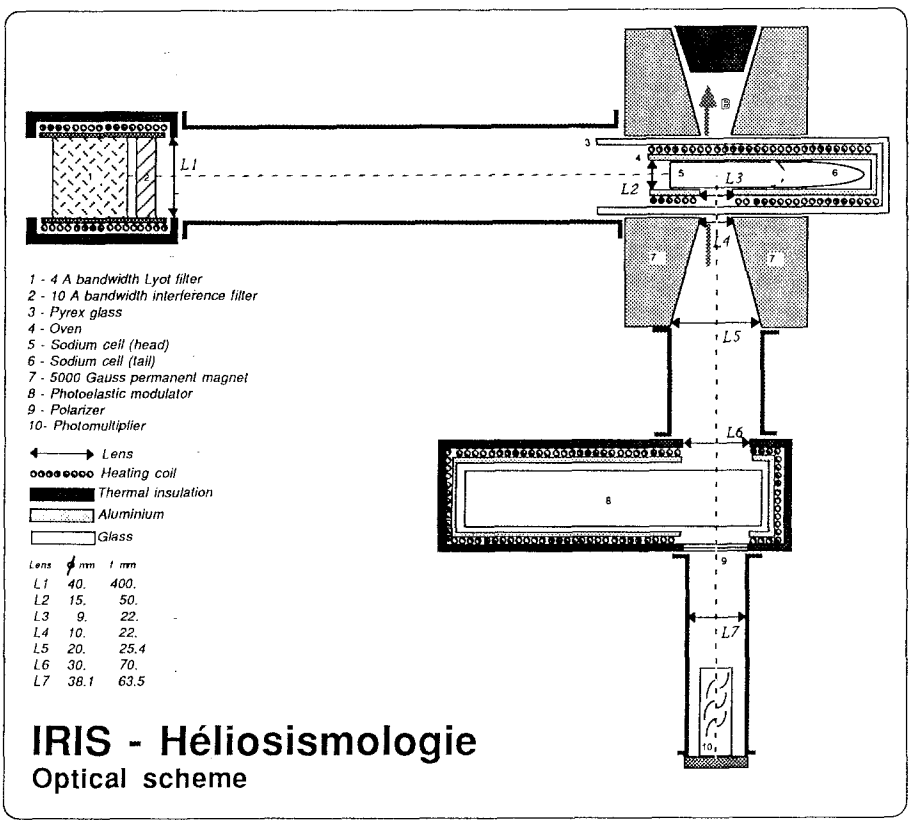

Fig. 2. Optical scheme of the IRIS instrument.

this solar image is rejected to infinity by a second lens (L2), which images the first one just inside the core of the sodium vapour located in the center of the transverse magnetic field.

After absorption, the scattered light is forwarded to the photomultiplier tube (PMT) by a series of 5 lenses. This number of lenses is justified by the need for some distance between the magnet and the PMT and the contradictory need for a wide angular

aperture of the light beam. Between the last two lenses is located the photoelastic modulator, which analyzes alternately and at a frequency of about 42 kHz the left and right circular polarizations produced by the two Zeeman components.

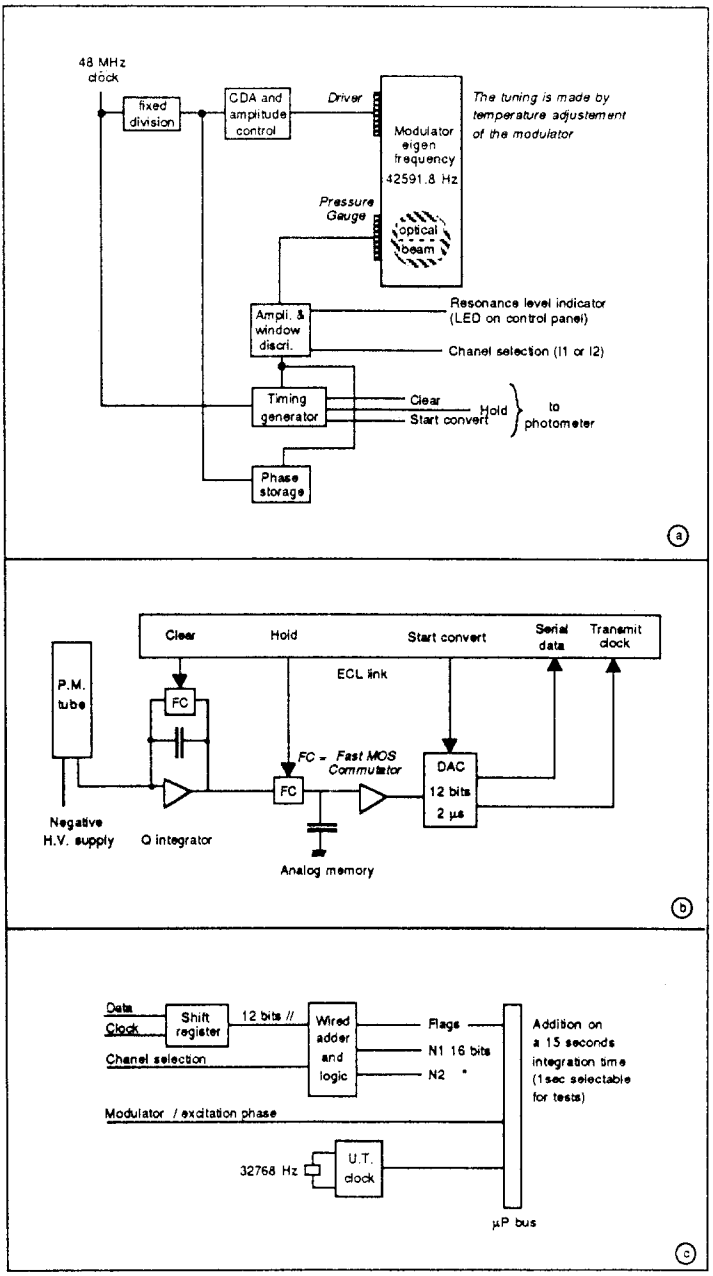

Fig. 3. Block diagram for the electronic data acquisition. (a) Photoelastic modulator control and phase synchronisation of measurements. (b) Photometric measurements and digitization. (c) Real-time data processing.

The PMT receives a light flux modulated at this frequency between the red and the blue wings of the D1 line. The mean flux of detected photons is in the range $3 \times 10^7\ s^{-1}$ to $4 \times 10^7\ s^{-1}$. The data acquisition system is included in a microprocessor unit which also contains a crystal-controlled time clock, the modulator driver, and the cassette tape recorder. This system outputs two analog lines used for a control display of the velocity signal together with the mean intensity signal on a two-channel chart recorder and two digital serial lines. One of these is used to send the time to the heliostat control, the second supports data exchange with a local computer, which can be used for local data storage and for time clock setting (this task can also be performed through an old-fashioned binary control panel).

The instrument is fed by a specific one-mirror heliostat. It consists of one flat mirror of square shape, 15 × 15 cm, located at a distance of the order of 4 m in front of the entrance window of the prefilter. In the northern hemisphere, the Sun travels in the southern part of the sky, and hence, the instrument is looking at the heliostat mirror in the northern direction. The altazimuth tracking is calculated by a second microprocessor unit, taking into account the geographical coordinates and the universal time. A photo-electric device detects the possible need for small corrections around the calculated mirror position, allowing errors in the final driving gears and in the setting relative to the local meridian and horizon: the trigonometrical computation assumes the heliostat's axis vertical and the reflected beam horizontal in the local meridian plane.

The third electronic rack is the analog thermal control unit. Four optical components are heated and temperature controlled. The two parts of the sodium cell (at temperatures of the order of 170 °C for the optical part and 153 °C for the tail which defines the vapour pressure). The prefilter and the modulator unit have sample-dependent nominal temperatures in the range 35 °C to 50 °C. The first component must be controlled within 0.5 °C, while the other three require a more severe control within less than 0.1 °C.

3. Theoretical Sensitivity

The various sources of the noise in the velocity signal are the Sun itself (as we have seen already), fluctuations of the sky transparency in front of the rotating Sun (Grec *et al.*, 1979), photon statistics and the instrument itself.

The power spectrum of the solar noise has been estimated by Harvey (1984) (Figure 4). Some experimental results obtained at Izaña (Jiménez *et al.*, 1986) have given to this model a good level of confidence. In good sky conditions, the sky noise happens to have the same order of magnitude with the same general frequency dependence. The general goal is then to maintain the photon statistics and the various instrumental noises below this solar noise level.

At first order the measured velocity signal is

$$V_s = V_0(I_R - I_B)/(I_R + I_B)\,,$$

where I_R is the solar flux in the red wing; I_B, the solar flux in the blue wing; the value of the sensitivity V_0 is related to the sodium line profile and to instrumental parameters: typically $V_0 = 5000\ m\ s^{-1}$.

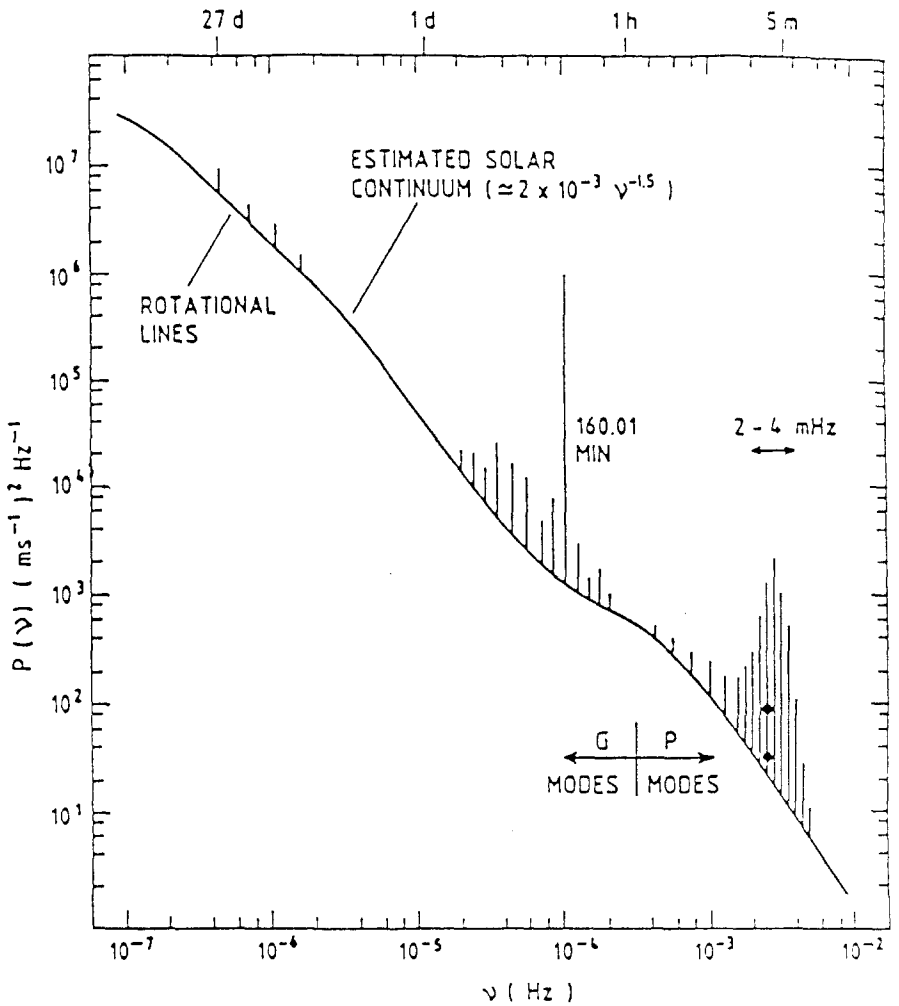

Fig. 4. (Harvey, 1985). Estimation of the background noise in the full disk Doppler measurements generated by granules, supergranules and magnetic activity on the solar surface. Assuming that most instrumental sources of noise will follow the same kind of frequency dependence, we impose for each component the specification of being a source of noise below this solar noise level in the limited frequency range in which it can be measured or reliably estimated (the high-frequency part).

We measure, in fact, the two numbers N_R and N_B, respectively for the two wings of the solar line:

$$N_R = G_R((1 - \varepsilon_R)T_R I_R + \varepsilon_R T_B I_B + d) + n\,,$$

$$N_B = G_B((1 - \varepsilon_B)T_B I_B + \varepsilon_B T_R I_R + d) + n\,,$$

where G_R and G_B are photometric efficiencies; ε_R and ε_B, cross efficiency factors for polarizers; d = non-resonant light, n, dark measurement; T_R and T_B, prefilter trans-

missions; using the ratios

$$\Gamma = G_R/G_B\,, \qquad \theta = T_R/T_B\,, \qquad \Omega = (N_R - N_B)/(N_R + N_B)\,,$$

we get

$$\Omega = \frac{I_R\Gamma\theta(1 - \varepsilon_R - \varepsilon_B/T) - I_B(1 - \varepsilon_B - \varepsilon_R\Gamma) + d(\Gamma - 1)}{I_R\Gamma\theta(1 - \varepsilon_R + \varepsilon_B/\Gamma) + I_B(1 - \varepsilon_B + \varepsilon_R\Gamma) + d(\Gamma + 1) + 2n}$$

and in the simplest case, where $T_R = T_B$, $G_R = G_B$, $\varepsilon_R = \varepsilon_B = \varepsilon$,

$$\Omega = [(1 - 2\varepsilon)/(1 + q)]\,[(I_R - I_B)/(I_R + I_B)]\,;$$

$1/q = (I_R + I_B)/(2d + 2n)$ is the resonance factor.

In this case the measured velocity V_I is related to the solar velocity V_s through

$$V_I = V_0\Omega$$
$$= (1 - 2\varepsilon)/(1 + q)V_s\,;$$

the photon noise can then be computed, using the variable $R = N_R/N_B$:

$$V_I = V_0(R - 1)/(1 + R)\,,$$
$$\mathrm{d}V_I = 2V_0/(R + 1)^2\,\mathrm{d}R\,,$$
$$\sigma^2(V_I) = \frac{4V_0^2}{(R + 1)^4}\,\sigma^2(R)\,,$$

N_R and N_B being independent random variables, proportional to the photon counting rate for each measurement:

$$\sigma^2(N_R) = N_R\,,$$
$$\sigma^2(N_B) = N_B\,,$$
$$\sigma^2(R) = R(R + 1)^2/N\,,$$
$$\sigma^2(V_I) = \frac{4RV_0^2}{(R + 1)^2}\,\frac{1}{N}\,.$$

Due to the orbital motion, $1 \leq R \leq 1.5$ and $0.96 < 4R/(R + 1)^2 < 1$. So that, using $N = N_R + N_B$, we obtain

$$\sigma^2(V_I) = V_0^2/N\,.$$

The photoelectron counting rate of $2.5 \times 10^7\ \mathrm{s}^{-1}$ would imply a relative statistical noise of 2×10^{-4}, or $1.0\ \mathrm{m\,s}^{-1}$ in a 1 s integration time, resulting in a flat noise of $1\ \mathrm{m}^2\,\mathrm{s}^{-2}\,\mathrm{Hz}^{-1}$ in the power spectrum. That can be satisfactorily compared with the solar noise displayed in Figure 4. In the integration time of 15 s which is used in the IRIS raw data, the photon noise is then expected to be of the order of $0.25\ \mathrm{m\,s}^{-1}$. Figure 5 shows how realistic this estimation is.

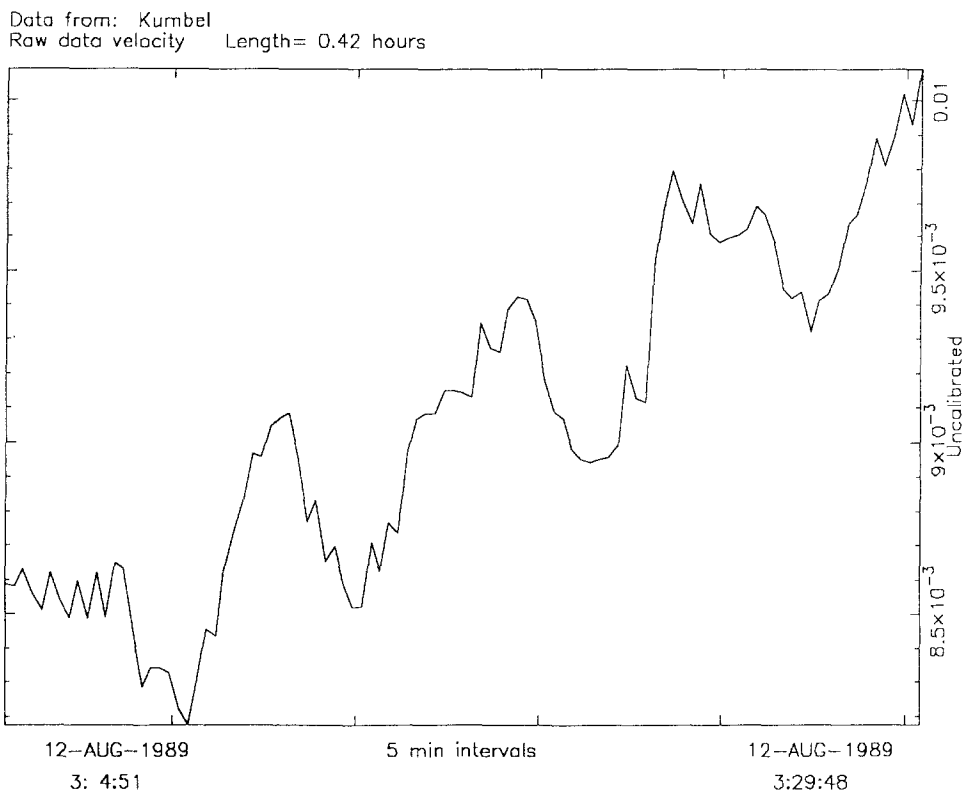

Fig. 5. In this example of about 25 min of IRIS data, the photon noise is clearly visible, with a r.m.s. value of the order of 25 cm s^{-1}, consistent with the photon counting rate in the sampling time of 15 s. The resulting contribution in the power spectrum is the bottom line of the frame box in Figure 4.

4. Critical Components and Specific Requirements

We shall see now how each component of the instrument could specifically reduce its global performance as compared with the estimated and measured photon noise and the specific requirements that have to be met. In most cases, the noise generated by an optical or an electronic component is frequency dependent, with a f^{-1} or a f^{-2} law, or something intermediate in the frequency range of interest, for periods between a few minutes and a few months. The noise spectrum of each component is then very similar to the solar or to the telluric one. It is then easy to investigate each contribution just by a comparison with the photon noise level in the sampling time of 15 s, the guide-line for instrumental design being to maintain this contribution well below the 25 cm s^{-1} of the photon statistics.

Using the variables already defined, and assuming the approximations q and ε small compared to 1, Γ, and θ close to 1, we get:

$$dV_I = -2V_s\, d\varepsilon\,,$$

$$dV_I = -V_s\,dq\,,$$

$$dV_I = 2V_0R/(R+1)^2\,d\theta/\theta\,,$$

$$dV_I = 2V_0R/(R+1)^2\,d\Gamma/\Gamma\,,$$

these differentials governing the noise in velocity versus the random variations of the instrument's parameters.

4.1. Heliostat and guiding accuracy

In solar Doppler-shift measurements, the signal is due not only to the local motions that we are looking for, but also to the global line-of-sight velocity between the instrument and the solar surface. This velocity is changing mostly with the rotation of the Earth and the Sun. On the Sun, the gradient is linear in the angular east-to-west direction, by about 2 m s^{-1} per each arc sec. Due to this value, any velocity measurement on a resolved solar image is highly sensitive to tracking errors. The difficulty is lower for full disk measurement: in that case the velocity integrated over the whole visible hemisphere is much less sensitive to the motions of the solar image on the instrument. This sensitivity to what is called offset guiding is minimized by imaging the entrance pupil in the resonant volume of the sodium vapour and by rejecting the solar image to infinity. A residual effect cannot be completely eliminated, due to the other optical components, and to the small variations of the exact volume of vapour participating in the measurement, just before and just after the pupil image along the entrance beam. This effect has been carefully measured by scanning the Sun on the Stanford IRIS instrument (Figure 6). The gradient appears to be of the order of 3 to 3.5 cm s^{-1} per arc sec, well below the imaged solar gradient.

Our tracking system calculates the position and moves the mirror each sec., with a mechanical resolution of 0.5 arc sec. This guiding accuracy is adequate compared to the 6 arc sec accuracy necessary to maintain the contribution of the noise below the photon noise in the sampling time-scale of 15 s. On the other hand, the computed position may differ from the real one due to the uncertainties in the positioning of the instrument and to periodic gear errors. Those drifts are amplitude-limited, thanks to a photoelectric device, detecting the visibility of four orthogonal parts of the limb out of a circular mask. Due to the variable size of the Sun, this device has a variable resolution, but when properly adjusted can detect 10 to 15 arc sec errors. On a longer time-scale, some image drift is possible, mostly due to the changing ellipticity of the solar image generated by the atmospheric differential refraction, and to the variation of the solar brightness offsetting the reference position of the photoelectric sensors. If this produces the usual aperiodic f^{-1} to f^{-2} spectrum, it will stay under the solar noise level. We cannot exclude there the possibility that some gear periodicity in the driving device will show up above the solar noise level in the velocity signal. However, the example published by Ehgamberdiev *et al.* (1991) is essentially noise limited and does not leave room for this effect.

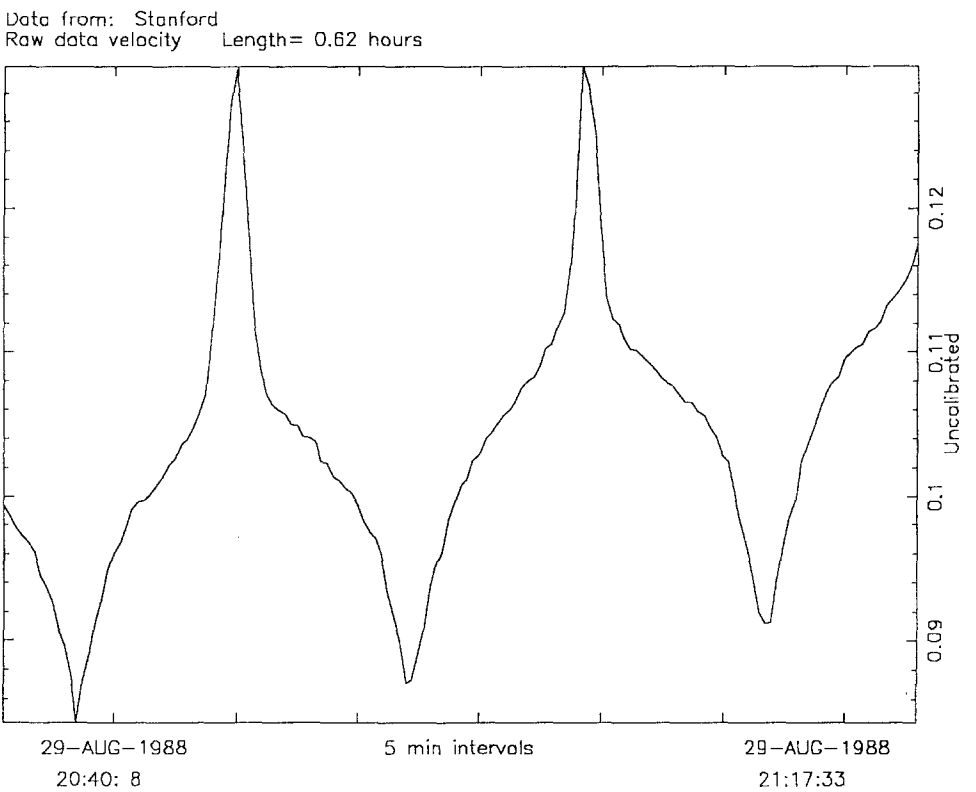

Fig. 6. Several scans of a complete solar diameter in amplitude are displayed. The central parts make it possible to measure the offset guiding sensitivity in the east/west direction. It is of the order of 3.5 cm s^{-1} per arc sec.

4.2. PREFILTER

This is a combination of a 10 Å interference filter and a one-layer calcite Lyot filter, the latter providing a sinusoidal transmission adjusted to be zero at the D2 5890 Å wavelength and maximum at D1 5896 Å.

The velocity measurement is differential between two points distant by $\frac{1}{30}$ of the filter bandwidth. In the case of a displacement of this bandwidth, the measurement is affected by the second derivative of its profile and by the resulting misbalance of the transmission on the two spectral windows of the sodium cell. The two filter components are temperature sensitive. The interference filter drifts to larger wavelength when heated, the retardation plate drifts in the opposite direction, due to changes in thickness and differential refraction inexes. Those effects compensate partially, leading us to foresee a global drift in the range of 4 to 10 m s^{-1} per 1 °C change in temperature. This sensitivity has been measured for 2 different filters, in the laboratory with a sodium spectral lamp and a white light source through the complete instrument, and on the Sun for a coronal day at Oukaïmeden. The results are a sensitivity of 4.5 ms^{-1} K^{-1} for the first filter, 10 ms^{-1} K^{-1} for the second. These 2 numbers are consistent with the above estimate.

Following our guideline on experimental errors, the temperature has to be controlled within 0.05 °C to maintain its contribution to the noise below the photon statistics level. In this case, we do not have easy access to the filter temperature on the short time scale of 15 s. Inside its housing it has a typical thermal time scale of 15 to 20 min, which is 60 to 80 times the sampling interval. At this scale, the temperature control accuracy should be better than 0.4 °C (assuming a f^{-1} frequency dependence on the power). The best we can say here is that the temperature fluctuations measured in 20 min never exceed 0.1 °C, so that the filter should not contribute significantly to the noise in the data.

4.3. Permanent magnet

Made of 4 individual samarium–cobalt magnets and a soft iron circuit, it provides inside a 22 mm air-gap an induction of the order of 4.9 kG (Figure 7). This value has been

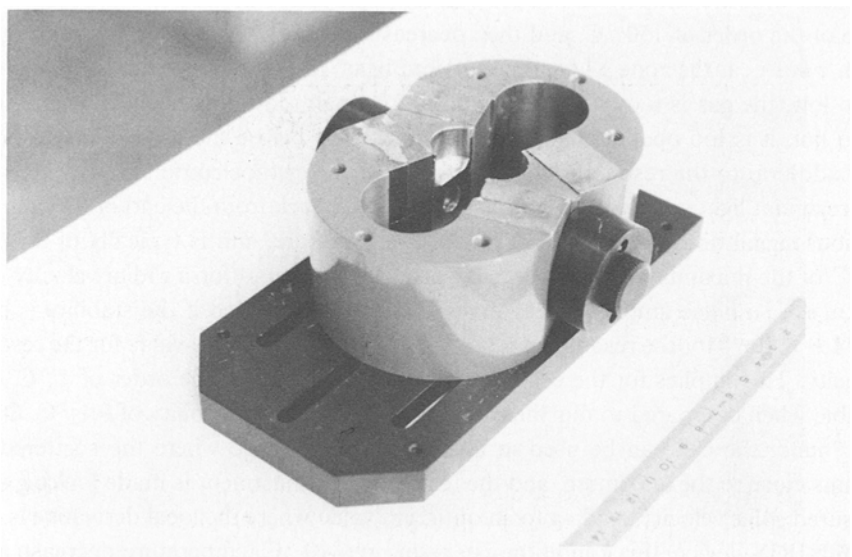

Fig. 7. This permanent magnet, designed for the IRIS instrument, gives a constant induction of 4.9 kG orthogonal to the incoming beam, in a 22 mm wide air-gap.

chosen for locating the two spectral windows on the steepest part of the D1 line profile.

The magnetic field value can change with the magnet temperature and with the effect of magnet aging. Once again, this will result in a noise of the f^{-1} type. At first sight, it seems that a change of the magnetic field value will induce only a second-order effect in the differential velocity measurement. However, the instrument is operated during a significant fraction of the time quite far from balance of the two channels, because of the gravitational redshift superimposed on the Earth spin and orbital motions. The slopes on the red and blue line wings can be, in this case, as different as 25%.

The samarium–cobalt magnet has a negative temperature coefficient of 4×10^{-4} for

reversible changes of magnetisation. This means that our magnetic field will change by about 2 G per 1 °C, inducing, in the case of the maximum misbalance quoted before, a velocity effect of the order of 50 cm s^{-1} per 1 °C. The magnet temperature, then, is not allowed to vary randomly by more than 0.5 °C on a time scale of 15 s. Here again, the temperature time constant of the magnet is longer, also of the order of 15 to 20 min, during which the temperature should not change by more than a few °C.

The magnet is ventilated in order to avoid excess heating due to the relatively high temperature of the sodium cell located in the air-gap. However, turning on the cell will still change the magnet temperature, within an hour or so, by at least 10 °C. It is then a general rule not to turn off the heating of the optical part of the cell at night, in order to insure that the magnet temperature effects can be neglected.

4.4. The sodium cell

The amount of light scattered by the sodium vapour and which reaches the PMT increases with the temperature of the coldest point inside the cell to a maximum for a value of the order of 150 °C, and then decreases again. This value leads to an optical depth $\tau = 1$ near the zone where the scattered beam is observed: when the temperature is too low, the gas is too transparent and not enough scattering occurs; when the gas is too hot, it is too opaque and the light is scattered before the optical side window.

In addition to the resonant light, a fraction of the photoelectric signal comes from non-resonant light scattered in the glass or reflected back from the end of the cell. This spurious signal does not depend on the cell temperature, and is typically of the order of 3% of the maximum resonant intensity. In this case, and for a radial velocity up to 1.5 km s^{-1}, a noise amplitude less than 25 cm s^{-1} is reached if the stability is better than 1.6×10^{-4} for the resonance ratio, i.e., 5×10^{-3} in relative value for the resonant intensity. This implies for the cell's temperature a stability of the order of 1 °C, comfortable when compared to our thermal control providing a stability of 0.1 °C. On the other hand, the cell can be used in a relatively wide range where the scattered flux remains close to the maximum, and the temperature adjustment is made looking at the measured solar velocity, leading to an optimum value where the local derivative is zero. For the IRIS device, this condition can result in a 10 °C temperature decrease and a 10% intensity loss compared to the maximum resonance. A numerical analysis of this effect has to take into account the solar line curvature, the radial velocity and the shape of the resonant lines in the cell, leading to results similar to our experimental determination (Boumier, 1990).

The cell heating is made in two separately controlled sections: the stem contains the liquid sodium whose temperature governs the sodium vapour pressure and thus the resonant intensity; the optical part of the cell is at a 20 °C higher temperature in order to avoid sodium condensation on the optical windows.

Another issue with the sodium cell is the glass aging. Originally, the cells were made of pyrex, which slowly reacted chemically with the hot sodium gas. This reaction resulted in a progressive darkening of the pyrex, which would loose half of its trans' parency in a time-scale of a few weeks to a few months, strongly temperature dependent.

The pyrex has been replaced by a specific glass from Schott, the lifetime of which is now well over one year. A new series of cells using the glass selected for the GOLF helioseismometer included in the SOHO project (Gabriel *et al.*, 1988) is also foreseen, having an as yet unknown limit in lifetime, and no detectable aging effects over two years of tests at a nominal temperature.

4.5. The modulator

So far, a good photometric measurement is possible only by means of a unique photon detector, with a modulation system making it possible to measure alternately the two channels. This makes it mostly insensitive to variations of amplification. In the case of our instrument, the optical modulator, which has to chop between right handed and left handed circular polarizations, must be transparent, must accept a wide angular aperture, and must be rapid enough to avoid an undersampling of atmospheric transparency fluctuations, which would introduce another source of noise while suppressing the first one.

The above requirements lead to the choice of the photoelastic modulator (Kemp, 1970; Canit and Badoz, 1983) in which a piezoelectric crystal excites the mechanical resonance of a piece of glass. This glass becomes birefringent under the effects of internal pressure gradients. The resonant frequency is close to 42 kHz for the selected size of the glass.

The birefringence is a sinusoidal function of time, and the transmission of one circularly polarized component is a sinusoidal function of the birefringence. A nearly square modulation is obtained for an optimum amplitude of the presssure variations. The intensity is measured on each chanel over 70% of each half wave, resulting for the velocity signal in a sensitivity equal to 0.95 of the ideal square modulation (Figure 8). Two piezo-electric crystals are glued on the resonant piece of glass, along the nodes of the mechanical resonant pattern. One is excited at a constant frequency, and the tuning is made by control of the modulator's temperature. The second piezo is used as a phase reference (at 90 degrees phase lag from the excitation) for synchronization of each individual measurement. The resonant frequency has a strong dependence of 2.8 Hz C^{-1}, due to the thermal expansion of the glass. It is also quite sharp, the FWHM of the response to a constant excitation being 3.8 °C (these two values are the results of our laboratory measurements). In addition, optical measurements have shown a zero phase lag between the mechanical polarization effect as measured by the instrument.

There are three main possibilities for this modulation system to be a source of noise in the velocity measurement. The individual integration gate timing can be noisy, resulting in a misbalance of the time of integration of the two intensities. The modulator temperature can change, thus resulting in a departure from optimum mechanical resonance. Finally, the amplitude of the mechanical resonance depends on the amplitude of the driving signal. In all cases, the result of any change of the working point will be a variation of the coefficient (0.95) of modulation. If the mean line-of-sight velocity is near zero, it will only produce a small change of velocity sensitivity, seen as a slight

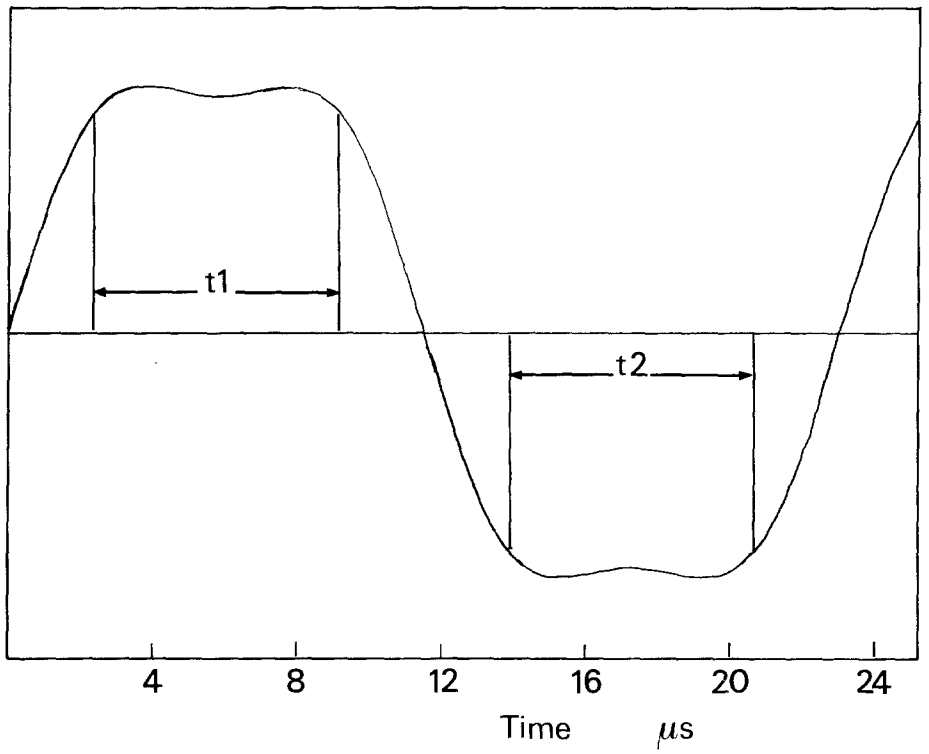

Fig. 8. The photoelastic modulator, when optimized in amplitude, provides this shape of modulation between the two circularly polarized components of the optical resonance. The integration intervals $t1$ and $t2$, respectively used for the measurement of the intensity in red and blue wings, are defined as shown by an electronic gating. This arrangement makes it possible to obtain a rate of modulation of more than 95%, as compared to the ideal case of a square modulation.

amplitude modulation of the solar oscillations. But in general, as we have already seen, the line-of-sight velocity has a large offset.

If we take 1 km s^{-1} as a typical offset value for the definition of the modulator specifications, then the modulation factor must be stable within 2×10^{-4} to insure a noise level lower than the photon statistics. The time of integration of each modulated sample is, for both channels, of the order of 8 μs. During the sampling time of 15 s, we have 6.3×10^5 such individual measurements added up. Following the above specification, we need to have a random noise not larger than 1.6 ns in the mean opening and closing times, integrated over 15 s. Given the large number of modulation periods during these 15 s, the individual commands could be noisy at the 1 μs level. In the IRIS device, a 48 MHz quartz oscillator is used to generate the driving signal for the modulator, and the timing of each measurement is derived from the same clock and from a zero-crossing detection of the signal coming from the auxiliary piezo, resulting in noise in the individual integration time in the 10^{-9} s range, far below the acceptable limit. The thermal drifts of the quartz frequency and of any delays in logical circuits are without effect on velocity

measurements, resulting in slow drift of the common photometric gain for the two channels.

Assuming a constant excitation amplitude, the rate of modulation will be a function of the temperature of the modulator, which defines its resonant frequency. Figure 9 shows this rate as a function of the variations around the ideal temperature in the ideal

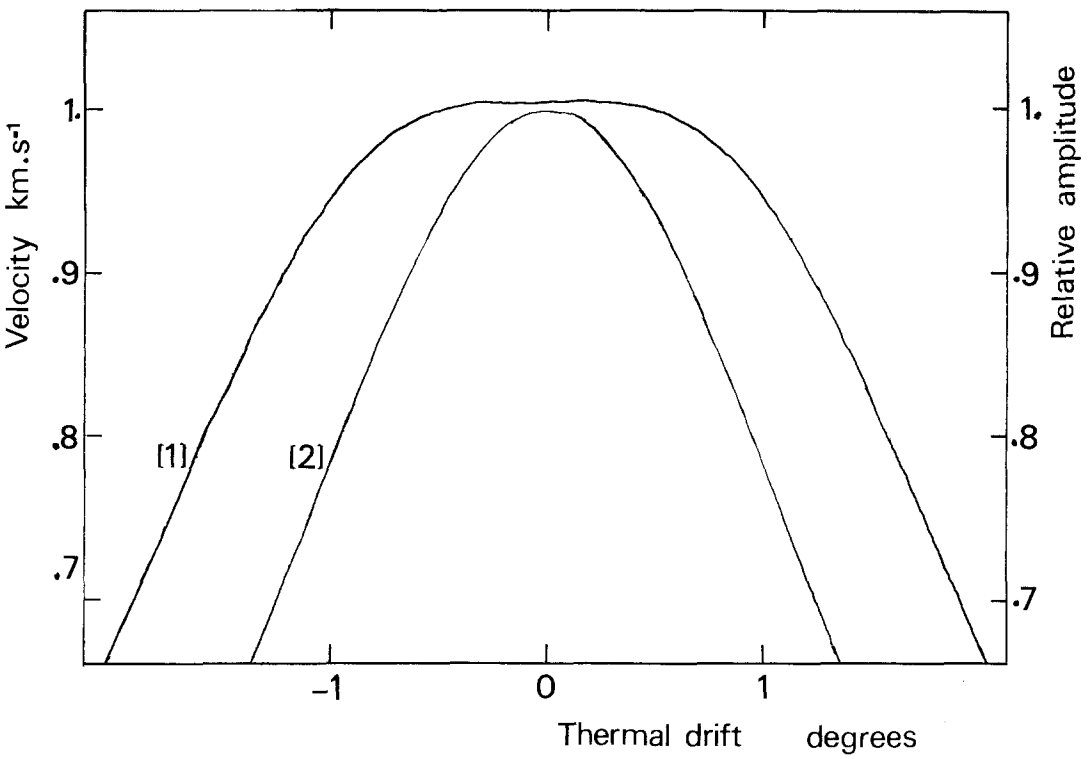

Fig. 9. Driven by an electrical signal at constant frequency and constant amplitude, the modulator has a temperature sensitivity described by the mechanical response curve [2] (right-side scale). This results in a decrease of the modulation factor with a thermal drift, and thus in a change of the measured velocity, described by the curve [1] (left-side scale), where we assume a 1 km s^{-1} radial velocity offset and an optimum amplitude adjustment.

case of an optimized excitation amplitude. One can see that control of the temperature within ± 0.15 °C is necessary to fulfill the modulation stability requirement. If the temperature is not in this range around its optimum value, then the problem becomes much more severe. With 1 °C offset, 10^{-3} °C would be necessary for maintaining the required modulation stability.

It has proved too difficult to constrain the modulator temperature inside the ± 0.15 °C range. The reason for that is the impossibility to have a heater very close to the resonant piece of glass, and the required optical apertures for incoming and outgoing light, which are sources of heat exchange; the excitation signal itself is also in thermal

balance. To accommodate small thermal drifts, the excitation level is controlled in real time, using the auxiliary piezo signal as input, in order to maintain a constant resonance level. In this case, the required accuracy in the amplitude control is defined by the second curve shown in Figure 9, and is in the range of 1%. However, we should allow the possibility for this amplitude not to be set at its precisely optimized value. A few percent error in this adjustment, which is made on the Sun separately for each instrument, may result in a factor 2 in the required control accuracy. Our experience is that the amplitude can be relatively easily adjusted within 1% in good sky conditions. In that case the automatic amplitude control accuracy, better than 0.5%, will do the job. In addition, due to electrical limitations, the thermal range in which the automatic amplitude control can be effective is narrower than 1 °C and a careful initial adjustment has still to be done.

An independent analysis of the noise generated by this modulation system has been made by P. Hoyng (this issue), leading to comparable results.

4.6. The preamplifier and the data acquisition system

The photometer is presently running under a maximum photo-pulse counting rate equal to $4 \times 10^7\ s^{-1}$. This value, necessary to reach an adequate photon noise level, is far too high to use a photon counting system. Therefore we have to use an analog device, locked in phase with the modulator. In the present design the photomultiplier's intensity is integrated over one-half of the modulator cycle in a capacitor; the result, obviously a voltage, is memorised in a hold device and digitized thanks to a 12 bit A–D converter; the integrator is cleared and the next integration begins before the 2 μs conversion. This system is fully synchronised with the mechanical resonance of the modulator, the dead time corresponding to the useless part of the modulation cycle. Such a measurement is made twice per cycle and transmitted to the microprocessor, where an additive input circuitry reduces the data flow by a factor 15 to a manageable level. The red and blue wing intensities are then averaged in 15 s intervals on 32 bit unsigned integers and stored in a stack, together with the time read at the end of the integration. The memory buffer is written on tape every 30 min, and for control display, the velocity is computed for each 15 s integration period.

We have seen in the previous section that the timing errors in the commands of individual measurements could not provide a significant contribution to the noise level. In this case, only the offset variations can be a source of concern. There are several electronic offsets coming from amplifiers and converters, added to the photomultiplier dark current. The total is generally of the order of a few 10^{-3} of the total intensity. Once again, it would only produce a small variation of sensitivity if the mean velocity was near zero, and the offset variations would be essentially negligible. In the same typical case of a mean velocity of about 1 km s^{-1}, the offset variations should not be more than 2×10^{-4} times the mean value of the two intensities. This happens to be about 1 mV.

The photomultiplier dark current amounts to a few mV, and will never change by as much as 1 mV in the time-scale of 15 s. On the other hand, the measurements of the offset voltage have shown slow variations of the order of a few mV in a few hours, which

are consistent with our specifications, but have also shown discontinuities up to 8 mV in case of power failure. These can contribute to the noise at a level higher than the photon statistics. In order to reduce this effect, it is necessary to implement a real-time measurement of the preamplifier offset, to be sampled during the measurements and recorded on tape files. This implementation is presently foreseen, as well as trials for better electronic stability. The alternative choice of a photon-counting device is also possible, but should require operation at a lower counting rate.

5. Conclusions

After many years of step-by-step improvements, our IRIS sodium cell spectrophotometer has now become a reliable instrument, able to provide full disk Doppler shift measurements only limited by the solar or the atmospheric noise in the whole period range comprised between years and minutes. The photon noise and each possible source of instrumental noise are maintained below these two sources in all cases, which comprise the *g*-mode and the *p*-mode frequency ranges. This is illustrated in the paper by Baijumanov *et al.* (this issue), where is shown a typical power spectrum obtained with one day of August 1989 Kumbel data.

The success of the IRIS network programme will then depend upon the long term reliability of the various instrumental components and also on the will of the observers, who must observe every clear day during more than a decade, who must carefully notice and report any problem, frequently check the instrument clock to insure an internal consistency of the time between all instruments, and more... Then will come the rest of the story, with the scientific programme to be developed with this data, and to be started with the optimization of the low-frequency quality of the data, or in other words by the optimal solution to the data merging problem. It must be noted that this topic, which is specific to the network data, is important for both the IRIS and GONG communities, which have already started efficient cooperation.

Our instrument design and performance was used as a model for the definition of the so-called GOLF spatial helioseismometer, to be flown in 1995 with the SOHO mission of the European Space Agency. This experiment, with a two year planned life, and a foreseen duration over four more years, will provide us with observations free from atmospheric perturbations and from diurnal effects.

Acknowledgements

The IRIS instruments are built with the help of many individuals in the scientific and technical staffs of various institutes. The heliostats are due to G. Mugnier, G. Pen, and A. Baldit. The prefilters have been designed and built by J. Demarcq. The magnets were designed by J. M. Robillot and built by A. Escobar. The sodium cells are due to C. Hallier and their housing to G. Rouget, who also built the modulators. The mechanical supports were designed by A. Robini, B. Bertin, and G. Galou and built by the mechanical shop of Bagnères de Bigorre. The main electronic parts are designed and built in our laboratory, with the participation of J. F. Manigault.

References

Baijumanov, A. *et al.*: 1991, *Solar Phys.* **133**, 51 (this issue).
Blamont, J. E. and Roddier, F.: 1961, *Phys. Rev. Letters* **7**, 437.
Boumier, P.: 1990, private communication.
Brookes, J. R., Isaak, G. R., and Van der Raay, H. B.: 1978, *Monthly Notices Roy. Astron. Soc.* **185**, 1.
Canit, J. C. and Badoz, J.: 1983, *Appl. Optics* **22**, 592.
Ehgamberdiev, S., Khalikov, S., Fossat, E.: 1991, *Solar Phys.* **133**, 69 (this issue).
Fossat, E.: 1970, Thèse de Spécialité, Université de Nice.
Fossat, E.: 1975, Thèse de Doctorat, Université de Nice.
Fossat, E.: 1984, *Mem. Soc. Astron. Ital.* **55**, 47.
Fossat, E. and Roddier, F.: 1971, *Solar Phys.* **18**, 204.
Fossat, E. and Ricort, G.: 1973, *Solar Phys.* **28**, 311.
Gabriel, A. H., Bocchia, R., Bonnet, R. M., Cesarsky, C., Christensen-Dalsgaard, J., Damé, L., Delache, P., Deubner, F. L., Foing, B., Fossat, E., Fröhlich, C., Gorisse, M., Gough, D. O., Grec, G., Hoyng, P., Pallé, P. L., Paul, J., Robillot, J. M., Roca Cortés, T., Stenflo, J., Ulrich, . K., and van der Raay, H. B.: 1988, *ESA Booklet on the SOHO Experiments.*
Grec, G.: 1981, Thèse de Doctorat, Université de Nice.
Grec, G., Fossat, E., and Vernin, J.: 1976, *Astron. Astrophys.* **50**, 221.
Grec, G., Fossat, E., and Pomerantz, M. A.: 1980, *Nature* **288**, 541.
Grec, G., Fossat, E., and Pomerantz, M. A.: 1983, *Solar Phys.* **82**, 55.
Grec, G., Fossat, E., Brandt, P., and Deubner, F. L.: 1979, *Astron. Astrophys.* **77**, 347.
Harvey, J.: 1984, in W. Noyes and R. K. Ulrich (eds.), *Probing the Depths of a Star*, NASA.
Hoyng, P.: 1991, *Solar Phys.* **133**, 43 (this issue).
Jiménez, A., Pallé, P. L., Pérez Hernandez, F., Régulo, C., and Roca Cortés, T.: 1986, *Astron. Astrophys.* **192**, L7.
Kemp, J. C.: 1970, *J. Opt. Soc. Am.* **59**, 950.
Roddier, F.: 1965, *Ann. Astrophys.* **28**, 463.
Snider, J. L.: 1970, *Solar Phys.* **12**, 352.